Article

Cell Stem Cell

GRHL2-Dependent Enhancer Switching Maintains a Pluripotent Stem Cell Transcriptional Subnetwork after Exit from Naive Pluripotency

Graphical Abstract

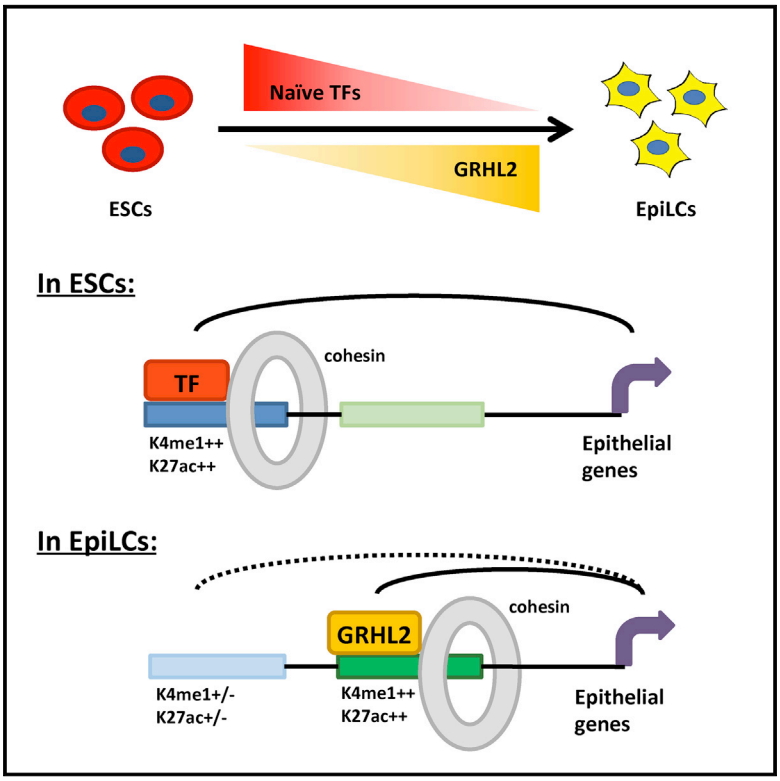

Highlights

- GRHL2 binds and activates enhancers during the transition from ESCs to EpiLCs
- GRHL2 maintains rather than activates target gene expression in EpiLCs
- GRHL2 target genes are regulated by distinct ESC-specific enhancers in ESCs
- GRHL2 loss results in an epithelial to mesenchymal-like transition in EpiLCs

Authors

Amy F. Chen, Arthur J. Liu, Raga Krishnakumar, Jacob W. Freimer, Brian DeVeale, Robert Blelloch

Correspondence

robert.blelloch@ucsf.edu

In Brief

Extensive epigenetic reprogramming occurs during the transition from naive ESCs to formative EpiLCs. Blelloch and colleagues show that the transcription factor GRHL2 rewires a subset of enhancers during the transition without altering cognate gene expression. By doing so, GRHL2 subdivides the naive pluripotency network prior to lineage diversification.

Chen et al., 2018, Cell Stem Cell *23*, 226–238
August 2, 2018 © 2018 Elsevier Inc.
https://doi.org/10.1016/j.stem.2018.06.005

CellPress

CellPress

Cell Stem Cell
Article

GRHL2-Dependent Enhancer Switching Maintains a Pluripotent Stem Cell Transcriptional Subnetwork after Exit from Naive Pluripotency

Amy F. Chen,[1,2] Arthur J. Liu,[2] Raga Krishnakumar,[1,2] Jacob W. Freimer,[1,2] Brian DeVeale,[1,2] and Robert Blelloch[1,2,3,*]
[1]The Eli and Edythe Broad Center of Regeneration Medicine and Stem Cell Research, Center for Reproductive Sciences, University of California, San Francisco, San Francisco, CA 94143, USA
[2]Department of Urology, University of California, San Francisco, San Francisco, CA 94143, USA
[3]Lead Contact
*Correspondence: robert.blelloch@ucsf.edu
https://doi.org/10.1016/j.stem.2018.06.005

SUMMARY

The enhancer landscape of pluripotent stem cells undergoes extensive reorganization during early mammalian development. The functions and mechanisms behind such reorganization, however, are unclear. Here, we show that the transcription factor GRHL2 is necessary and sufficient to activate an epithelial subset of enhancers as naive embryonic stem cells (ESCs) transition into formative epiblast-like cells (EpiLCs). Surprisingly, many GRHL2 target genes do not change in expression during the ESC-EpiLC transition. Instead, enhancers regulating these genes in ESCs diminish in activity in EpiLCs while GRHL2-dependent alternative enhancers become activated to maintain transcription. GRHL2 therefore assumes control over a subset of the naive network via enhancer switching to maintain expression of epithelial genes upon exit from naive pluripotency. These data evoke a model where the naive pluripotency network becomes partitioned into smaller, independent networks regulated by EpiLC-specific transcription factors, thereby priming cells for lineage specification.

INTRODUCTION

During mammalian development, pluripotent cells that have the ability to generate all cells of an organism arise with formation of the early epiblast at the time of implantation (Nichols and Smith, 2012; Rossant and Tam, 2009). Following implantation, epiblast cells undergo epigenetic, gene expression, and morphological changes while remaining pluripotent (Bedzhov and Zernicka-Goetz, 2014; Boroviak et al., 2015; Hayashi et al., 2011; Nakamura et al., 2016; Rastan, 1982). In mice, this transition from pre-implantation to post-implantation epiblast can be reproduced *in vitro* with the differentiation of embryonic stem cells (ESCs) to epiblast-like cells (EpiLCs) (Buecker et al., 2014; Hayashi et al., 2011; Krishnakumar et al., 2016). Reporter systems distinguishing the two cell states have enabled near-homogeneous reproduction of this transition (Buecker et al., 2014; Krishnakumar et al., 2016; Parchem et al., 2014).

ESCs maintained in the presence of leukemia inhibitory factor (LIF) and inhibitors to GSKβ and MEK (2i) are transcriptionally similar to cells of the E4.5 pre-implantation epiblast and are commonly called naive ground state pluripotent stem cells (Boroviak et al., 2015; Nichols and Smith, 2009). EpiLCs arise during ESC differentiation 2–3 days following removal of 2i+LIF, with or without addition of fibroblast growth factor 2 (FGF2) and activin (Buecker et al., 2014; Hayashi et al., 2011; Krishnakumar et al., 2016). EpiLCs are transcriptionally similar to cells of the E5.5 post-implantation epiblast and have been called primed pluripotent cells as they represent a homogeneous population of cells that are about to undergo lineage specification with the initiation of gastrulation (Hayashi et al., 2011; Nakamura et al., 2016). However, more recently, they have been renamed formative pluripotent cells to differentiate them from primed epiblast stem cells (EpiSCs) (Smith, 2017), which more closely resemble anterior primitive streak cells *in vivo* (Kojima et al., 2014). The ESC to EpiLC transition provides a rare opportunity to study the molecular basis of an *in vivo* transition *in vitro* at near homogeneity.

The transition from naive to formative pluripotency involves extensive epigenetic remodeling as cells prepare for lineage specification. Previous epigenetic studies in this transition have focused on changes in global DNA methylation levels, transcription factor (TF) localization and enhancer histone states (Auclair et al., 2014; Borgel et al., 2010; Buecker et al., 2014; Krishnakumar et al., 2016). However, enhancer activation also involves recruitment of architectural proteins such as the mediator and cohesin complexes (Kagey et al., 2010). Since enhancers can typically be located anywhere between 1 kb and 1 Mb from their target gene promoters (Calo and Wysocka, 2013), these complexes play a central role in anchoring 3D physical interactions between enhancers and their target gene promoters to drive gene expression (Kagey et al., 2010; Phillips-Cremins et al., 2013). Given the key role of these architectural proteins in regulating enhancer activity, we aimed to identify mechanisms regulating changes in enhancer activity during the naive to formative transition by examining changes in cohesin localization.

Here, we identify Grainyhead-like 2 (GRHL2) as a TF associated with cohesin localization during differentiation from ESCs to EpiLCs. GRHL2 activates enhancers during the transition to

EpiLCs. Interestingly, many GRHL2 target genes are already expressed in ESCs and are located near alternative ESC enhancers that are becoming inactivated in EpiLCs. Enhancer deletion experiments confirm that these genes switch from regulation by an ESC enhancer to a GRHL2-regulated enhancer during differentiation. These targets are enriched for epithelial and cell adhesion genes. Accordingly, GRHL2 loss results in an epithelial to mesenchymal-like transition in EpiLCs, but not ESCs. These findings show that GRHL2 assumes regulation of a subset of the larger naive network during differentiation to the formative state. It maintains expression of an epithelial program that is characteristic of both naive and formative pluripotency, as well as a subset of downstream lineages. We propose a model in which the large naive pluripotency network becomes partitioned into smaller networks regulated by distinct EpiLC TFs in the formative state, allowing the networks to be differentially regulated upon gastrulation.

RESULTS

OTX2 and GRHL2 Motifs Are Associated with Cohesin Relocalization during the ESC to EpiLC Transition

To follow changes in enhancer activation during the ESC to EpiLC transition, we used a previously established differentiation system where naive ESCs are differentiated into a near homogeneous population of formative EpiLCs (Krishnakumar et al., 2016). Principal-component analysis of the expression profiles of these *in vitro* cell populations with those in the pre- and post-implantation epiblast showed that our ESCs and EpiLCs closely resemble their *in vivo* counterparts (Figure S1A). Using this system, we examined cohesin localization in the two states by performing chromatin immunoprecipitation sequencing (ChIP-seq) for the cohesin core subunit SMC1 and identifying SMC1 binding sites relative to an immunoglobulin G (IgG) control. We identified 10,705 ESC sites and 12,690 EpiLC sites using the MACS2 software package with a false discovery rate (FDR) < 0.05 (Zhang et al., 2008). Cohesin is found at insulator regions as well as enhancers (Kagey et al., 2010). To enrich for enhancers in our analyses, we depleted insulator sites by removing all sites co-bound by CTCF, a protein that is enriched at insulators and has relatively constant binding sites between cell types (Kim et al., 2007). Following subtraction of these sites (identified in Kagey et al., 2010), there remained 5,160 SMC1-bound sites in ESCs and 5,563 sites in EpiLCs, with many of these sites being distinct in the two states (Figure 1A; Table S1).

Esrrb and *Fgf5* represent genes that are specifically expressed in ESCs and EpiLCs, respectively. Therefore, we examined the genomic regions surrounding *Esrrb* and *Fgf5* during this transition (Figure 1B). In the region surrounding the naive marker, *Esrrb*, there were several SMC1 binding sites that were significantly enriched in ESCs relative to EpiLCs based on differential peak calling using MACS2. Conversely, there was an SMC1 binding site that was significantly enriched in EpiLCs relative to ESCs near *Fgf5*, a gene highly upregulated in the formative state. Together, these results suggest that our SMC1 ChIP-seq data reflect changing enhancer activity and that cohesin binding at enhancers is highly dynamic during the ESC to EpiLC transition.

Cohesin has no known sequence specificity and therefore is likely recruited either directly or indirectly to its binding sites by sequence-specific TFs. To identify candidate TFs that may recruit cohesin, we performed a motif enrichment analysis on EpiLC-specific SMC1 peaks using the Homer software package (Heinz et al., 2010). This analysis uncovered several motifs that were enriched in EpiLC-specific sites relative to the ESC-specific and common SMC1 sites. One of these enriched motifs was the binding motif for the TF OTX2 (Figure 1C). *Otx2* is upregulated during the ESC to EpiLC transition and plays an important role in re-localizing OCT4 (Buecker et al., 2014). qRT-PCR confirmed the upregulation of *Otx2* during this transition (Figure 1D). The motif for another TF, GRHL2, was also highly enriched in the EpiLC SMC1 peaks, and GRHL2 showed an almost 10-fold increase in expression with the ESC to EpiLC transition. GRHL2 belongs to the Grainyhead-like family of TFs, composed of GRHL1–3. These TFs have partially redundant roles in development (Boglev et al., 2011; Rifat et al., 2010). Unlike *Grhl2*, *Grhl3* is downregulated during ESC differentiation but relatively low in both states (Figure S1B). *Grhl1* is not expressed during this window. These findings identify GRHL2 as a potential regulator of changing enhancer activity during the ESC to EpiLC transition.

GRHL2 Binding Correlates with Nucleosome Removal, Acquisition of Active Histone Marks, and Cohesin Binding

Given the strong enrichment of the GRHL2 motif at EpiLC-specific SMC1 peaks, we next asked whether GRHL2 is binding these sites and, if so, what epigenetic events are associated with GRHL2 binding. To identify GRHL2 binding sites, we performed ChIP-seq for the endogenous GRHL2 protein in wild-type EpiLCs as well as GRHL2 KO EpiLCs as a background control. GRHL2 knockout (KO) EpiLCs were generated by CRISPR/Cas9-mediated mutagenesis of exon 2 of the *Grhl2* gene in ESCs followed by differentiation of the ESCs into EpiLCs. Homozygous null GRHL2 clones were identified by sequencing and western blot analysis (Figure S1C). When using an IgG ChIP in wild-type EpiLCs as a background control, we identified 1,686 significant GRHL2 peaks (FDR < 0.05), with ~60% of these sites containing a canonical GRHL2 motif. However, when using a GRHL2 ChIP in GRHL2 KO EpiLCs rather than IgG as the background control, we identified 332 peaks, with 86% containing a canonical GRHL2 binding motif (Table S2). The ChIP signal intensities at these peaks across two biological replicates were highly correlated (Spearman's correlation = 0.90; Figure 2A). Due to the much higher enrichment for the GRHL2 motif at peaks identified using GRHL2 KO cells as the background control, these sites were considered high confidence sites and used in all further downstream analysis. However, the same trends were observed with all peaks identified relative to IgG that contain the GRHL2 motif, as shown in matching supplemental figures.

Genomic annotation of GRHL2 binding sites showed that GRHL2 binds primarily at intergenic and intronic regions, consistent with a predominant regulatory role at enhancers as opposed to promoters (Figure 2B). This was further supported by the low levels of the promoter histone mark H3K4me3 at GRHL2 sites relative to active promoters (Figure S1D). Next, we asked what epigenetic changes occur with GRHL2 binding to these enhancer sites. Along with our SMC1 ChIP-seq data, we evaluated published H3K4me1 and H3K27ac ChIP-seq data performed under identical culture conditions

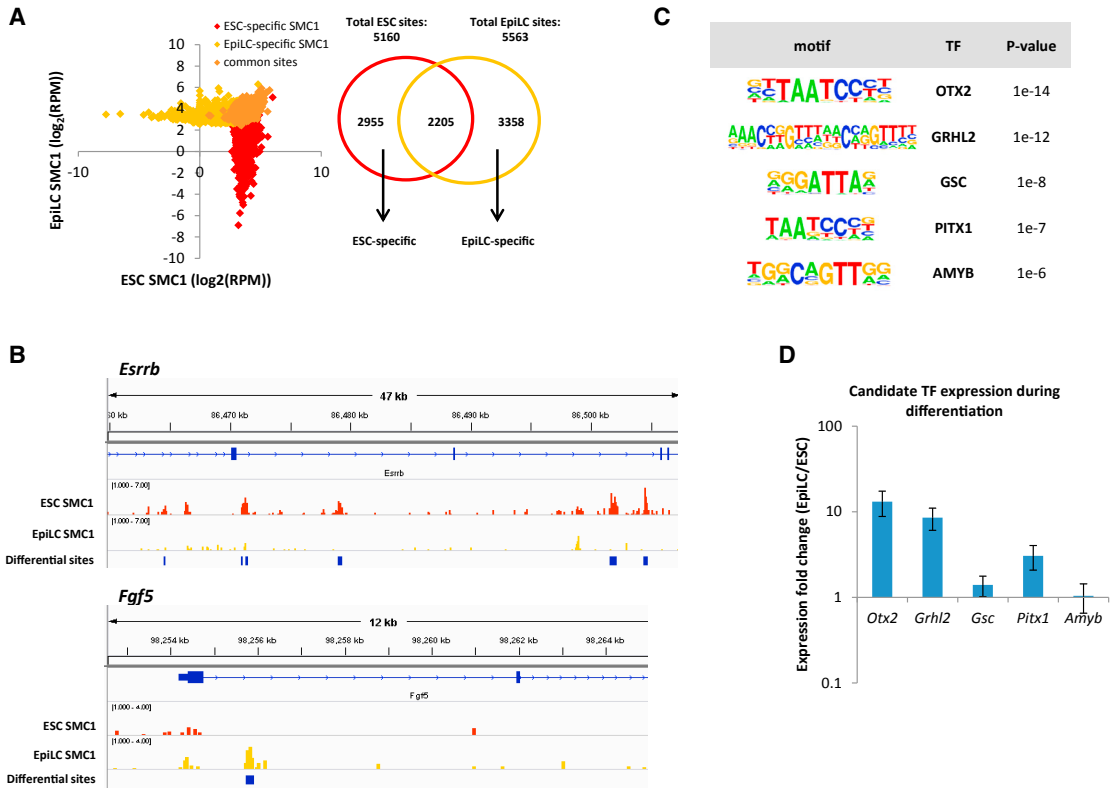

Figure 1. ChIP-Seq for SMC1 Identifies Candidate TFs that Regulate Cohesin Re-localization during the ESC to EpiLC Transition

(A) Left: SMC1 signal at ESC-specific, EpiLC-specific, and common SMC1 sites called with MACS2 (FDR < 0.05). To deplete insulators, sites co-bound by CTCF are not included. RPM, reads per million. Right: Venn diagram showing overlap of SMC1 sites in ESCs and EpiLCs. We identified 2,955 ESC-specific, 3,358 EpiLC-specific, and 2,205 common SMC1 sites.

(B) SMC1 ChIP-seq tracks at *Esrrb* and *Fgf5* genomic loci, with blue bars indicating significant differential peaks between ESCs and EpiLCs as called by MACS2.

(C) Top transcription factor motifs enriched at EpiLC-specific SMC1 sites, using all ESC SMC1 sites as a background.

(D) Expression fold change in EpiLCs versus ESCs for top 5 transcription factor candidates as quantified by qPCR. Error bars represent SD of n = 3 biological replicates. $p < 0.05$ for OTX2 and GRHL2 by Student's t test.

(Krishnakumar et al., 2016). We also performed an assay for transposase-accessible chromatin with high-throughput sequencing (ATAC-seq) to measure changes in nucleosome occupancy. A low ATAC-seq signal represents a nucleosome-occluded site, while a high signal represents the removal of nucleosomes (Buenrostro et al., 2013). Active enhancers were identified by the combination of high ATAC-seq, high SMC1, and high flanking H3K4me1 and H3K27ac signal (Buenrostro et al., 2013; Creyghton et al., 2010; Kagey et al., 2010; Rada-Iglesias et al., 2011). In ESCs, future GRHL2 sites showed low levels of all active enhancer marks, including low ATAC-seq and the absence of H3K4me1, H3K27ac, and SMC1 signals, indicating that these enhancers have little to no activity in ESCs (Figures 2C and 2D). In contrast, upon GRHL2 binding during the ESC to EpiLC transition, the same sites gained all marks of fully activated enhancers (high ATAC signal, H3K4me1, H3K27ac, and SMC1). This difference between ESCs and EpiLCs was diminished with increasingly lower-confidence GRHL2 binding sites (Figure S1E, IgG background with motif; and Figure S1F, IgG background without motif). Our findings were corroborated by H3K4me1 and H3K27ac ChIP-seq data from an alternative naive-to-formative differentiation system (Figures S1G and S1H; Buecker et al., 2014). As a control, we found little change in these marks at SMC1 sites common to both states (Figure S1I). These results indicate that GRHL2 binding correlates with full enhancer activation, suggesting a role for GRHL2 in the regulation of not only cohesin binding but also other crucial steps in enhancer activation.

GRHL2 Is Necessary and Sufficient for Full Enhancer Activation

Given the strong association between GRHL2 binding and various events in enhancer activation, we asked whether GRHL2 binding is necessary for each of these events. To address this question, we assessed levels of each active enhancer mark in wild-type and GHRL2 KO EpiLCs by performing ATAC-seq and ChIP-seq for H3K4me1, H3K27ac, and SMC1. There was a strong reduction in all active enhancer marks (chromatin accessibility, H3K4me1, H3K27ac, and SMC1 levels) at GRHL2 sites in GRHL2 KO EpiLCs, suggesting a near complete block in enhancer activation in the absence of GRHL2 (Figure 3A and 3B). These effects were diminished with increasingly lower-confidence GRHL2 binding sites (Figure S2A, IgG background with motif; and Figure S2B, IgG background without

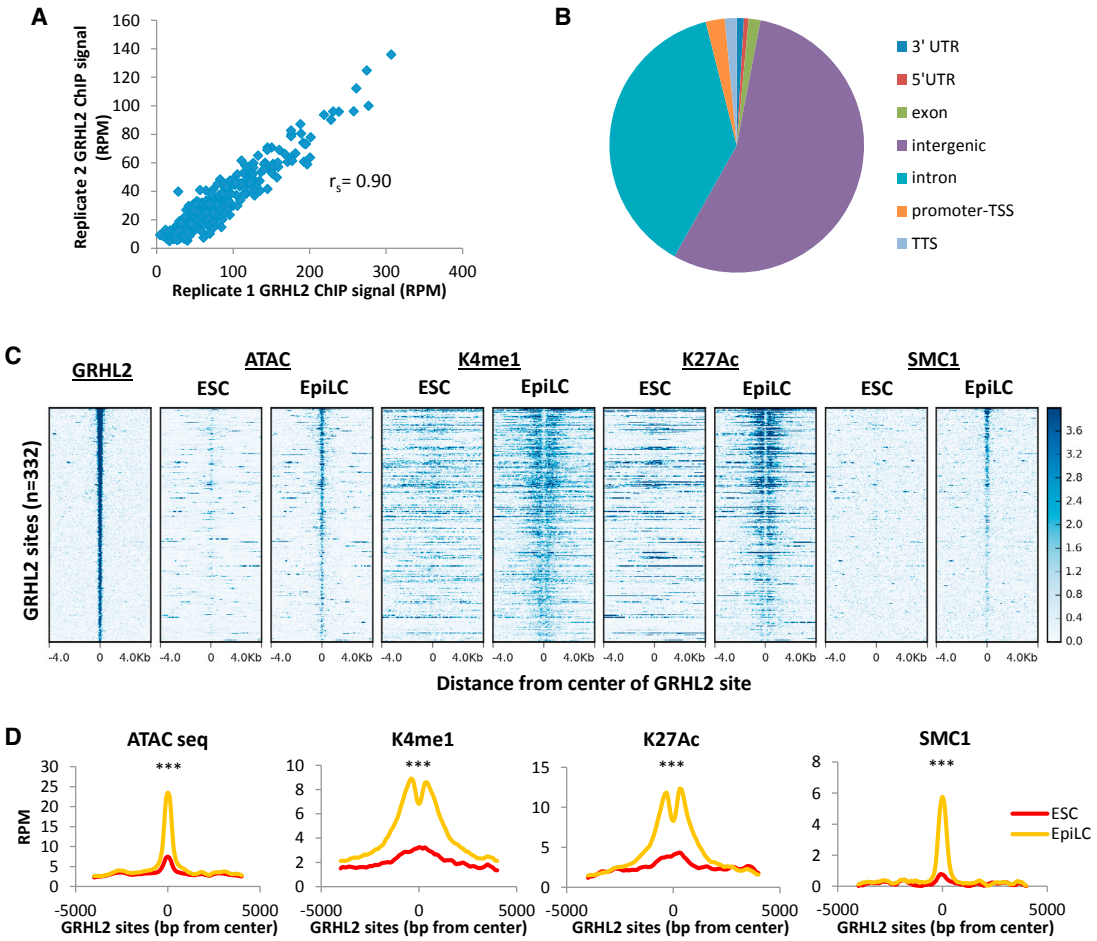

Figure 2. GRHL2 Binding Correlates with Nucleosome Removal and Full Enhancer Activation

(A) Average GRHL2 ChIP-seq signal for a 200-bp window surrounding GRHL2 sites in replicate 1 versus replicate 2, plotted as reads per million. Spearman's correlation = 0.90.

(B) Genome annotation of GRHL2 binding sites defined by UCSC mouse genome annotation v5.4.

(C) Heatmaps at EpiLC GRHL2 sites for enhancer marks in ESCs and EpiLCs. All plots are shown for an 8-kb window centered on GRHL2 binding sites. Sites are shown in descending order based on mean GRHL2 ChIP signal intensity.

(D) Metagene analysis of average signal across GRHL2 sites for heatmaps shown in (C). All plots are shown for an 8,000-bp window centered at GRHL2 binding sites. RPM, reads per million. K4me1 p = 1.36E-41; K27ac p = 6.80E-15; SMC1 p = 3.73E-34; ATAC-seq p = 2.78E-65 (paired t test).

motif). Loss of GRHL2 did not change levels of these marks at other cohesin sites gained during differentiation into EpiLCs (Figure S2C). Furthermore, the loss of marks was not secondary to a defect in differentiation, as common naive and formative markers were expressed at levels indistinguishable from wild-type during differentiation to EpiLCs (Figure S2D). Together, these results indicate an absolute requirement for GRHL2 for enhancer activation specifically at its target sites.

Since GRHL2 binding sites are nucleosome occluded in ESCs and lack all marks of enhancer activity, the full activation associated with GRHL2 binding suggests it is able to access closed chromatin to activate target enhancers during differentiation. If true, then ectopic expression of GRHL2 in ESCs should be sufficient to fully activate these enhancers. To test this, we generated two independent ESC lines containing *Rosa26*-M2rtTA and a doxycycline-inducible hemagglutinin (HA)-tagged *Grhl2* in the *Col1A1* locus (Figures S3A and S3B) (Beard et al., 2006). When treated with doxycycline, this resulted in a 60-fold overexpression of HA-tagged *Grhl2* in ESCs relative to endogenous EpiLC levels (Figure S3C). We performed ChIP-seq for HA and active enhancer marks (H3K4me1, H3K27ac, and SMC1) in untargeted and dox-inducible HA-GRHL2 ESCs, both of which were treated with doxycycline for 24 hr. The ectopically expressed GRHL2 protein was able to access and bind most endogenous GRHL2 EpiLC sites (Figure 3C; Table S3). These sites gained high levels of active enhancer marks (H3K4me1, H3K27ac, and SMC1) and had a marked depletion of nucleosomes at the center of histone peaks indicative of an active enhancer state (Figures 3D and 3E). Ectopic GRHL2 bound numerous additional ectopic sites, likely due to the high levels of expression associated with doxycycline induction. Interestingly, these ectopic sites also gained high levels of active enhancer marks with ectopic GRHL2 binding (Figure S3D), further supporting the ability of GRHL2 to access closed

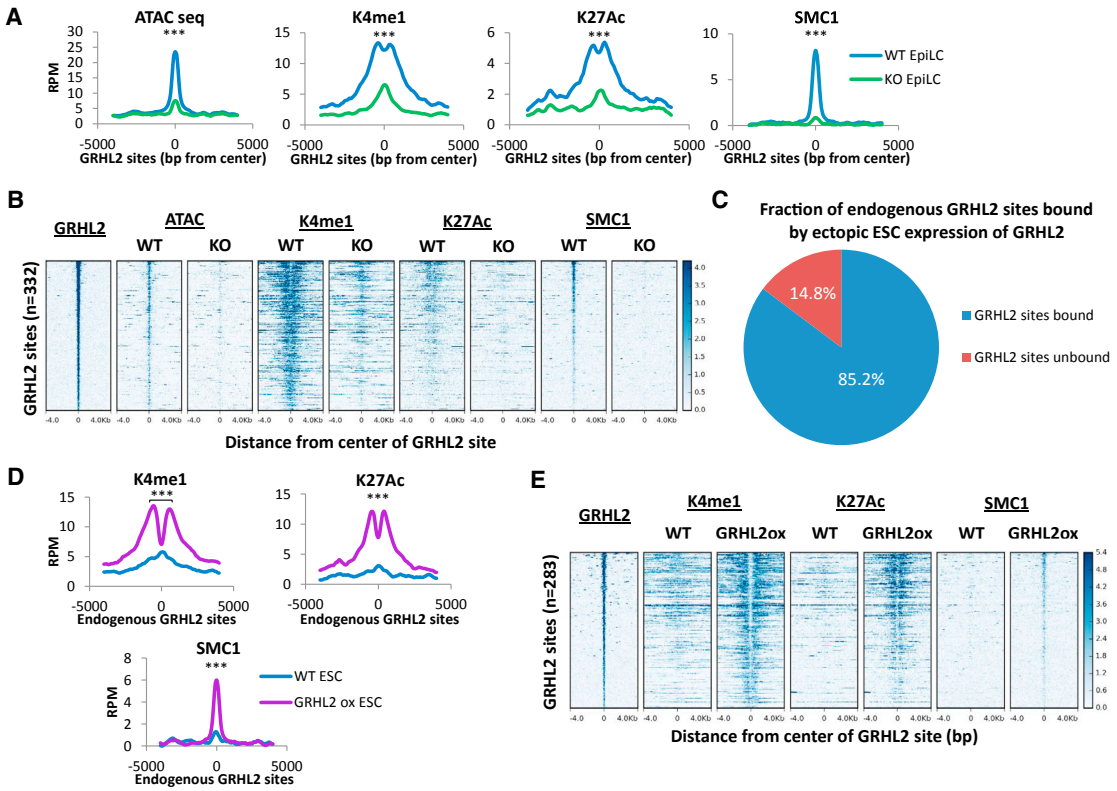

Figure 3. GRHL2 Is Necessary and Sufficient for Full Enhancer Activation

(A) Metagene analysis of average signal across GRHL2 sites in GRHL2 knockout and wild-type (V6.5) EpiLCs. All plots are shown for an 8,000-bp window centered on GRHL2 binding sites. RPM, reads per million. K4me1 p = 8.79167E-50; K27ac p = 1.77148E-52; SMC1 p = 3.08123E-40; ATAC: p = 7.13881E-72 (paired t test).

(B) Heatmaps at GRHL2 sites for enhancer marks in GRHL2 knockout and wild-type (V6.5) EpiLCs. All plots are shown for an 8-kb window centered on GRHL2 binding sites. Sites are shown in descending order based on mean GRHL2 ChIP signal intensity.

(C) Fraction of endogenous GRHL2 binding sites in EpiLCs that are bound by GRHL2 overexpression in ESCs (GRHL2 sites bound).

(D) Metagene analysis of average signal across endogenous GRHL2 sites that are ectopically bound in GRHL2 overexpressing ESCs in untargeted (WT) cells and dox-inducible GRHL2 ESCs, both treated with doxycycline. RPM, reads per million. K4me1 p = 1.56194E-45; K27ac p = 3.69415E-24; SMC1 p = 1.0148E-34 (paired t test).

(E) Heatmaps showing all individual loci in (D). All plots are shown for an 8-kb window centered on GRHL2 binding sites. Sites are shown in descending order based on mean GRHL2 ChIP signal intensity.

chromatin and fully activate target sites. To determine whether these results could be explained by differentiation of cells overexpressing GRHL2, we measured changes in expression of canonical naive and formative markers with 24-hr induction of GRHL2 expression in ESCs. There were minimal or no changes in expression of these markers, except for a 5-fold increase in the formative marker *Dnmt3b* (Figure S3E). The increase in *Dnmt3b* is likely due to direct regulation by GRHL2, as it is also significantly downregulated in EpiLCs upon GRHL2 loss (Figure S2D). Together, these results show that GRHL2 is not only necessary but also sufficient to bind and fully activate latent enhancers in the context of ESCs.

GRHL2-Regulated Genes Are Similarly Expressed during the Transition from Naive to Formative Pluripotency

Our finding that GRHL2 activates latent enhancers suggested that GRHL2 functions in transcriptional activation of its target genes. Therefore, we evaluated expression of predicted GRHL2 targets during the transition from ESCs to EpiLCs. Recent high-resolution chromatin interaction analyses in ESCs supports the use of nearest neighbor as an approximation of enhancer-target gene pairs at the genome-wide level, even though many exceptions occur at the individual gene level (Dowen et al., 2014; Schoenfelder et al., 2015). Studies have also shown that topologically associating domain (TAD) boundaries restrict enhancer activity to genes within the same TAD (Dowen et al., 2014; Ji et al., 2016). Therefore, we assigned enhancers to target genes that were the nearest gene within the same TAD. We used TAD boundaries previously identified in ESCs. These TAD boundaries were shown to be generally stable across different cell types (Dixon et al., 2012). The median distance between GRHL2-bound enhancers and the nearest gene within the same TAD was 27 kb, which is well within the range for a typical enhancer-promoter interaction (Figure S4A; Table S4) (Calo and Wysocka, 2013; Dowen et al., 2014). To evaluate whether GRHL2 drives expression of its predicted target genes, we performed expression profiling of 4 independent clones of

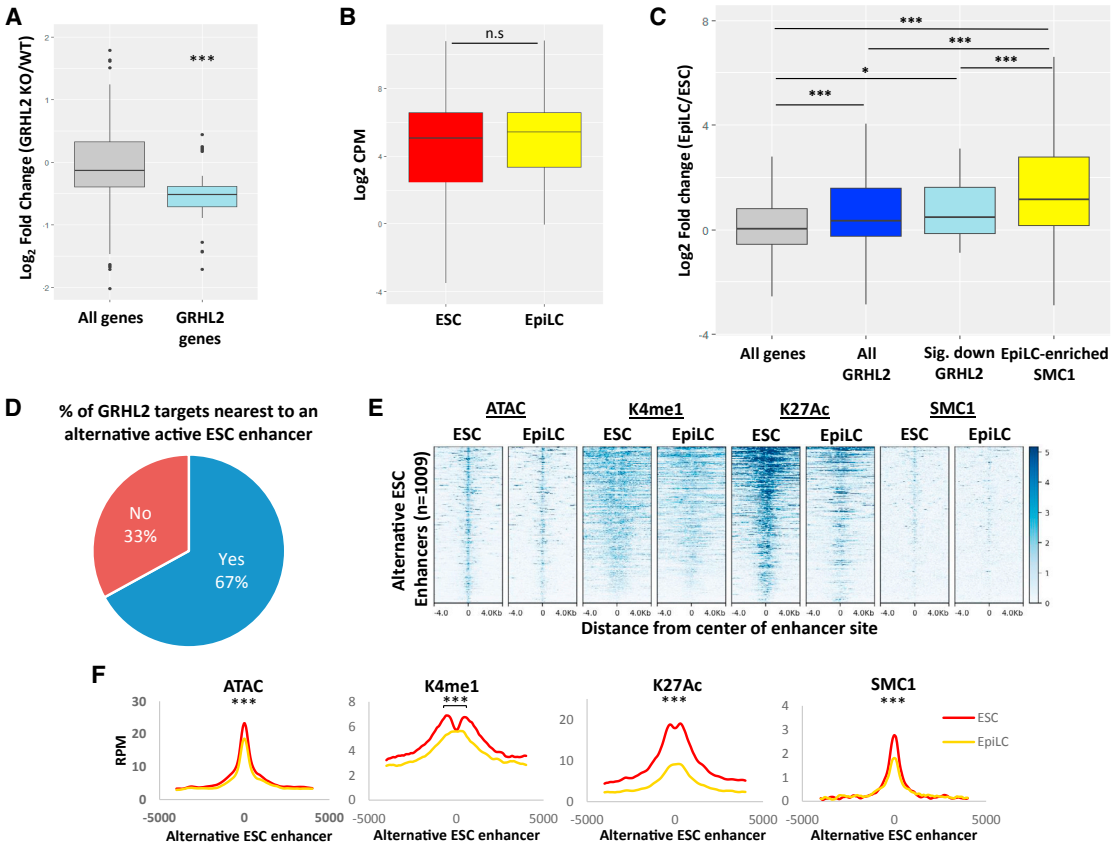

Figure 4. GRHL2 Target Genes Are Similarly Expressed during the ESC to EpiLC Transition and Are Regulated by Distinct Enhancers in ESCs

(A) Boxplots of expression changes in GRHL2 KO versus WT EpiLCs for all significantly changed genes (with adjusted p < 0.05) and all significantly changed genes nearest to GRHL2 sites, indicating a relative downregulation of GRHL2 targets in GRHL2 KO cells (p = 1.195E-9 by Mann-Whitney-Wilcoxon test).

(B) Boxplots showing distribution of expression for all candidate GRHL2 target genes in ESCs and EpiLCs based on RNA-seq data. CPM, counts per million.

(C) Boxplots of the log2 fold change in expression in EpiLCs versus ESCs for all genes, candidate GRHL2 target genes based on nearest neighboring gene within the same TAD, verified GRHL2 targets based on downregulation in GRHL2 KO cells, and candidate targets of EpiLC-enriched SMC1 sites. EpiLC-enriched SMC1 sites were identified relative to ESC SMC1 sites using bdgdiff in MACS2. *p < 0.05, ***p < 0.005 by Student's t test.

(D) Pie chart showing percentage of GRHL2 target genes in EpiLCs that are nearest to an alternative active enhancer in ESCs.

(E) Heatmaps for enhancer marks in ESCs and EpiLCs at the alternative ESC enhancers in (D). All plots are shown for an 8-kb window centered on the enhancer site. Note that multiple alternative enhancers exist per GRHL2 target, resulting in 1,009 alternative enhancers total.

(F) Metagene analysis showing average signal for the heatmaps shown in (E). A significant decrease in the levels of each active enhancer mark is observed (ATAC p = 2.59E-25; K4me1 p = 6.07E-09; K27ac p = 3.30E-59; SMC1 p = 5.50E-18 by paired t test). All plots are shown for an 8-kb window centered at the enhancer sites. RPM, reads per million.

wild-type and GRHL2 KO EpiLCs. Hierarchical clustering analysis separated GRHL2 KO from wild-type EpiLCs, showing a significant impact of GRHL2 loss on the transcriptome of these cells (Figure S4B). With GRHL2 loss, a similar number of genes were significantly up- and downregulated (1,016 genes upregulated and 1,020 genes downregulated; adjusted p value < 0.05), likely representative of both direct and indirect effects (Figure 4A; Table S5). Seventeen percent of the predicted GRHL2 gene targets were significantly changed upon GRHL2 loss. The predicted gene targets showing little to no change in expression could be due to any combination of incorrect target prediction, lack of probes that reliably detect these genes on the Illumina Bead array, and redundancy in gene regulation with other TFs. For those genes that did significantly change upon GRHL2 loss, over 80% were downregulated, consistent with GRHL2 being a transcriptional activator (Figure 4A).

Surprisingly, despite our results showing that GRHL2 activates latent enhancers and positively regulates expression of a number of its candidate target genes, we found that predicted GRHL2 targets were already expressed in ESCs at similar levels to EpiLCs (Figure 4B). While there was a slight average upregulation of predicted GRHL2 targets relative to all genes during the ESC to EpiLC transition, the magnitude of upregulation of GRHL2 targets was significantly less than the upregulation observed for all genes nearest to EpiLC-enriched SMC1 binding sites (Figure 4C). This remained true when focusing only on predicted GRHL2 targets that were significantly downregulated with GRHL2 loss in EpiLCs. The fact that there was a downregulation of GRHL2 targets in EpiLCs but little change in expression during the ESC to EpiLC transition suggested alternative mechanisms of regulation of these genes in ESCs. Using qRT-PCR, we confirmed that GRHL2 targets that are significantly

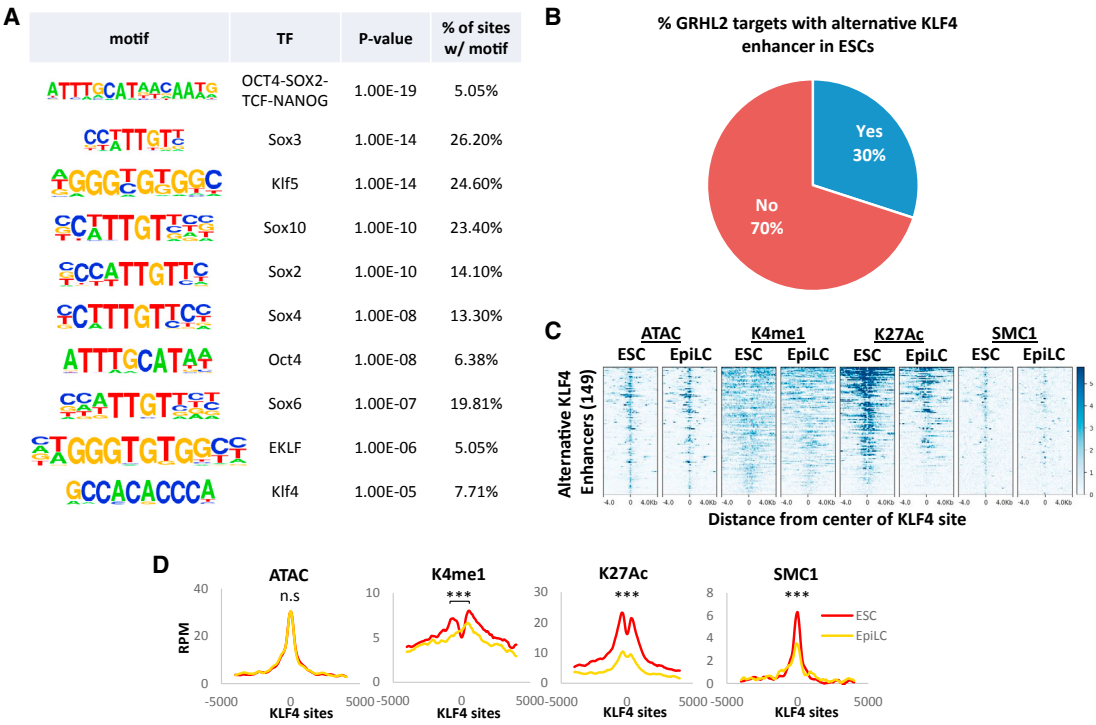

Figure 5. Pluripotency Transcription Factors Are Enriched at Alternative ESC Enhancers Near GRHL2 Targets

(A) Motif analysis at the alternative enhancers for GRHL2 targets in ESCs to identify candidate TF motifs that are enriched at these sites.

(B) Pie chart showing percentage of GRHL2 target genes in EpiLCs that are nearest to a KLF4-bound site in ESCs. KLF4 binding sites at promoters were excluded to enrich for enhancers.

(C) Heatmaps for enhancer marks in ESCs and EpiLCs at ESC KLF4 sites that have a GRHL2 target as its nearest gene. All plots are shown for an 8-kb window centered on KLF4 binding sites.

(D) Metagene analysis showing average signal for the heatmaps in (C). A significant decrease in signal in the EpiLC state was observed for each enhancer mark except for ATAC-seq signal. (K4me1 p = 2.81E-3; K27ac p = 4.83E-12; SMC1 p = 1.87E-10).

downregulated with GRHL2 loss in EpiLCs are regulated independently of GRHL2 in ESCs (Figures S4C and S4D). Together, these findings indicate that many GRHL2 target genes are positively regulated by GRHL2 in EpiLCs but show little change in the ESC to EpiLC transition, suggesting that they are regulated by other TFs in ESCs.

GRHL2-Regulated Genes Are Controlled by Distinct Enhancers in ESCs and Undergo an Enhancer Switch during Differentiation to EpiLCs

Given that GRHL2-induced enhancer activation during the ESC to EpiLC transition was required for transcriptional maintenance of neighboring genes rather than transcriptional activation, we next asked whether expression of these genes was driven by alternative enhancers in ESCs. To identify potential alternative enhancers that drive expression of GRHL2 target genes in ESCs, we looked for active enhancers in ESCs that are likely associated with these genes based on the enhancer having a GRHL2 target gene as the nearest gene within the same TAD (Figure S4E). We identified active ESC enhancers based on the presence of a significant ATAC-seq peak (FDR < 0.05) marked by both H3K4me1 and H3K27ac. We found such enhancers near 67% of predicted GRHL2 target genes, and almost all of these were at least 1 kb away from the GRHL2-bound site (Figure 4D; Table S6). These potential alternative ESC enhancers were a median distance of 42 kb away from the GRHL2 target gene (Figure S4F). Upon differentiation into EpiLCs, these enhancers exhibited small but significant decreases in the ATAC-seq signal, H3K4me1, and SMC1, along with a marked reduction in H3K27ac, consistent with the enhancers becoming inactivated during the transition (Figures 4E and 4F). Indeed, H3K27ac is generally thought to be one of the first marks lost during enhancer inactivation (Bogdanovic et al., 2012; Bonn et al., 2012). Since GRHL2-bound enhancers are becoming activated as these alternative ESC enhancers are becoming inactivated, these findings suggest that GRHL2-regulated genes undergo a switch in enhancer usage during the ESC to EpiLC transition, typically maintaining rather than altering gene expression.

To identify candidate TFs that regulate the predicted alternative ESC enhancers, we used Homer to identify enriched sequence motifs at these sites. The top hits included numerous pluripotency TF motifs (Figure 5A). Particularly intriguing was a motif common to several KLF TFs (KLF4, KLF5, and EKLF). The KLF TFs are rapidly downregulated as naive ESCs transition to the EpiLCs (Figure S2D). Using available KLF4 ChIP-seq data in ESCs grown in similar culture conditions (LIF+2i) (Liu et al., 2017), we found that 30% of GRHL2 targets in EpiLCs are the

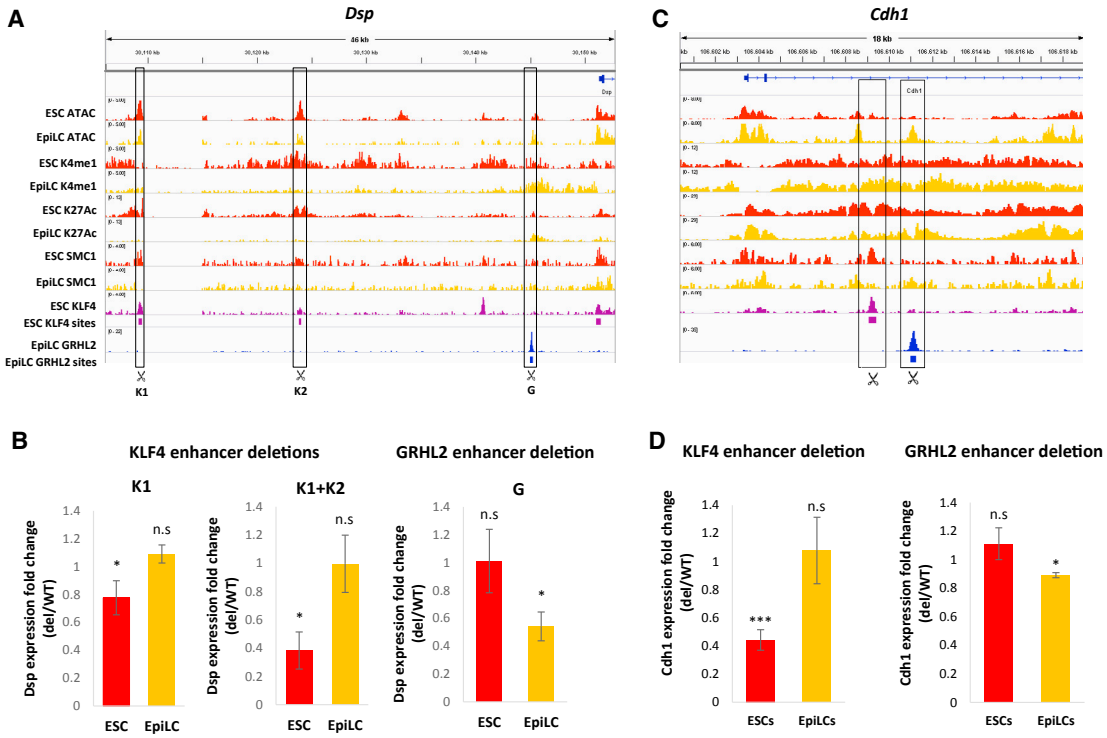

Figure 6. Functional Validation of Enhancer Switching at GRHL2 Target Genes during the ESC to EpiLC Transition

(A) ChIP-seq and ATAC-seq tracks in WT ESCs and EpiLCs at the *Dsp* locus, with significant KLF4 and GRHL2 binding sites indicated by purple or blue bars, respectively. KLF4 and GRHL2 sites deleted using CRISPR are indicated.

(B) Fold change in *Dsp* expression with deletion of the indicated KLF4 enhancers (K1 alone, or K1 and K2) or GRHL2 enhancer in ESCs and EpiLCs. *$p < 0.05$ by Student's t test. Error bars indicate SD for n = 3 biological replicates.

(C) Same as in (A) but for the *Cdh1* locus.

(D) Fold change in Cdh1 expression with deletion of the nearby KLF4-bound enhancer (left) or GRHL2-bound enhancer (right) in ESCs and EpiLCs. *$p < 0.05$ and ***$p < 0.005$ by Student's t test. Error bars indicate SD for n = 3 biological replicates.

nearest neighbor to a KLF4-bound enhancer in ESCs (Figure 5B; Table S6). The median distance between the KLF4-bound enhancer and GRHL2 target promoter was ~29 kb (Figure S5A). Almost all of these KLF4-bound enhancers were at least 1 kb away from the GRHL2 enhancer sites, indicating that they are distinct enhancers. These enhancers showed reduced H3K4me1, H3K27ac, and SMC1 during differentiation, consistent with their inactivation just as the GRHL2-bound sites become activated (Figure 5C and D).

To further test whether GRHL2 targets are regulated by the KLF TFs in ESCs, we generated double-knockout (DKO) ESCs for KLF2 and KLF4 (Figure S5B). However, RNA sequencing (RNA-seq) analysis showed that while many of these targets were changed in expression, there were a similar number that were upregulated and downregulated (Figure S5C). The lack of preferential downregulation of GRHL2 targets could be a result of secondary effects from the constitutive nature of the knockouts, as well as compensation by other KLF proteins. Therefore, we decided to take an alternative approach and directly delete the enhancer binding sites for GRHL2 and KLF4 at several of the target genes.

To delete the TF binding sites, we used CRISPR/Cas9-mediated editing to generate ~200-bp deletions surrounding the KLF4 or GRHL2 sequence motif at the bound sites near three target genes: desmoplakin (*Dsp*), E-cadherin (*Cdh1*), and junctional adhesion molecule 1 (*Jam1*). At the *Dsp* locus, there were two KLF4 binding sites and one GRHL2 binding site near the *Dsp* promoter (Figure 6A). We generated ESC lines with deletions for one of the two KLF4 sites (K1), both KLF4 sites (K1+K2), or the GRHL2 site (G). We then assessed the effects of each enhancer deletion on *Dsp* expression in ESCs and EpiLCs by qRT-PCR. If a true enhancer switch occurs between the KLF4-bound and GRHL2-bound enhancers during the ESC-to-EpiLC transition, then the enhancer deletions should only affect expression of *Dsp* in the state in which they are supposedly active. Indeed, we found that deletion of one or both KLF4-bound enhancers led to a significant reduction in *Dsp* expression in ESCs but had no effect in EpiLCs (Figure 6B). Conversely, deletion of the GRHL2-bound enhancer resulted in significantly reduced *Dsp* expression in the EpiLC state but had no effect in ESCs (Figure 6B). We observed similar state-specific reductions in target gene expression with deletions of the KLF4-bound and GRHL2-bound enhancers at the *Cdh1* and *Jam1* loci (Figures 6C, 6D, S6A, and S6B). While these deletions could potentially remove binding motifs of other TFs, the loss of active enhancer marks with GRHL2 loss and the gain of these marks with ectopic binding of GRHL2 strongly suggest a direct role for GRHL2 in regulating these enhancers. Together,

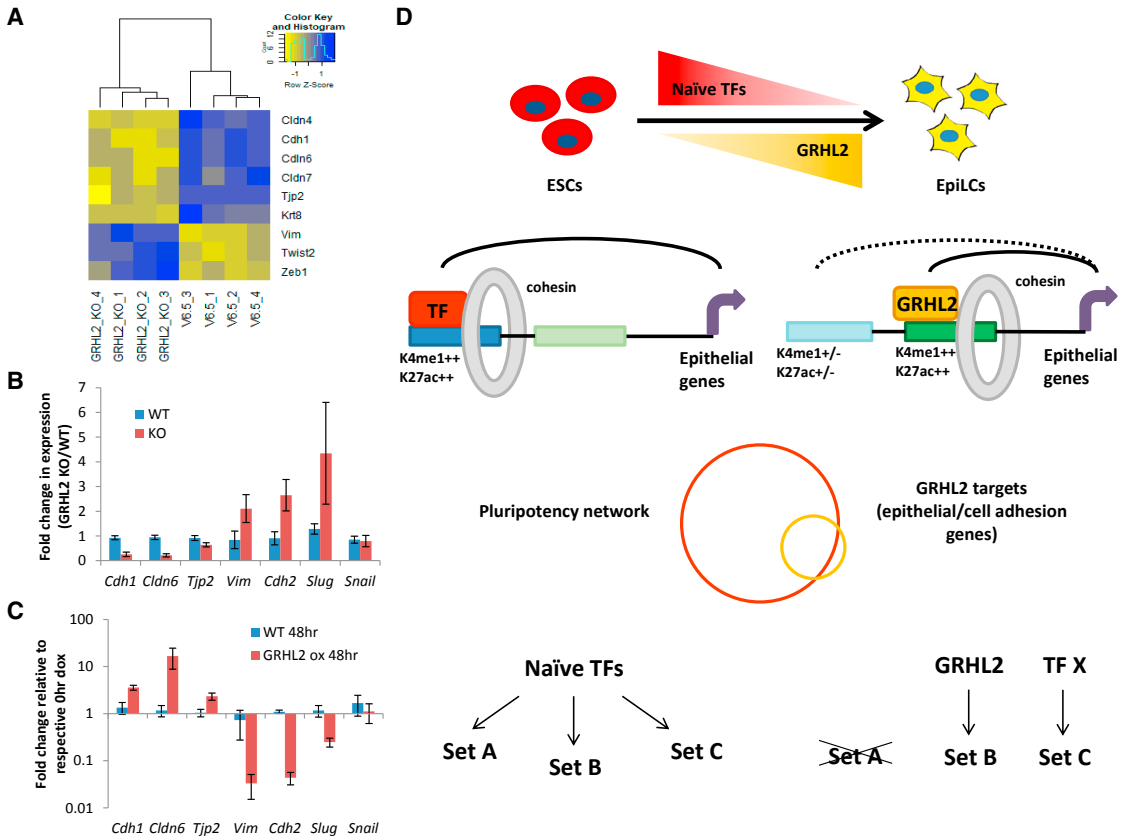

Figure 7. GRHL2 Loss Prevents Maintenance of the Epithelial Expression Program and Results in EMT of EpiLCs

(A) Clustered heatmap of common epithelial and mesenchymal markers that are significantly changed (adjusted $p < 0.05$) in 4 independent clones of GRHL2 KO EpiLCs versus WT (V6.5) EpiLCs.

(B) qPCR validation of expression changes for epithelial (*Cdh1*, *Cldn6*, and *Tjp2*) and mesenchymal (*Vim*, *Cdh2*, *Slug*, and *Snail*) markers in WT (V6.5) versus GRHL2 KO EpiLCs. Error bars show SD for n = 4 biological replicates. $p < 0.05$ for all markers except *Snail* by t test.

(C) Expression of epithelial and mesenchymal markers in WT and dox-inducible GRHL2 overexpressing ESCs treated with doxycycline for 0 or 48 hr as quantified by qPCR. Expression is normalized to respective 0-hr doxycycline samples for each cell line. Error bars indicate SD for n = 3 biological replicates. $p < 0.05$ for all markers except *Vim* ($p = 0.056$) and *Snail*.

(D) A model where naive-specific pluripotency factors including the KLF TFs regulate a broad repertoire of genes in ESCs, many of which need to be maintained in the formative state. TFs upregulated in the formative state activate new enhancers to maintain expression of these genes while the ESC-specific enhancers become inactivated. In the case of GRHL2, the target genes promote an epithelial state characteristic of both naive and formative pluripotent cells. We speculate that other EpiLC-specific TFs regulate additional subsets of the larger naive network.

our results show that expression of these GRHL2 target genes is maintained during the ESC to EpiLC transition via an enhancer switch that is regulated by the KLF and GRHL2 TFs.

GRHL2 Suppresses an Epithelial to Mesenchymal Transition in EpiLCs

Next, we examined the biological role of enhancer switching at GRHL2 target genes. As expected, GRHL2 KO ESCs did not have any obvious morphological phenotype under self-renewal growth conditions, since GRHL2 expression is low or undetectable at this stage (Figure S7A). However, upon differentiation to EpiLCs, unlike wild-type cells, KO cells did not remain in compact colonies. Genomic regions enrichment of annotations tool (GREAT) analysis of GRHL2-regulated enhancers showed enrichment for basolateral plasma membrane, cell-cell junction, and apical junction complex genes characteristic of an epithelial state (Figure S7B) (McLean et al., 2010). These ontology groups were also among the top enriched terms when performing gene ontology (GO) analysis of genes nearest to GRHL2 enhancers using Enrichr (Figure S7C) (Chen et al., 2013; Kuleshov et al., 2016). These data suggested that GRHL2 is maintaining expression of genes specifically involved in promoting an epithelial state and cell adhesion in EpiLCs.

To test the role of GRHL2 in maintaining EpiLCs in an epithelial-like state, we measured several markers of both the epithelial and mesenchymal states. Consistent with morphological changes, microarray data showed a decrease in epithelial markers and a gain in mesenchymal markers with GRHL2 loss (Figure 7A). qRT-PCR confirmed the downregulation of the epithelial markers *Cdh1*, *Cldn6*, and, to a small degree, *Tjp2*. In contrast, the mesenchymal markers, *Vim*, *Cdh2*, and *Slug* were upregulated (Figure 7B). The overexpression of *Grhl2* in ESCs led to an opposite result, with the same markers showing altered expression in the opposing direction (Figure 7C). With the

exception of *Cldn6,* these markers do not normally change with the ESC to EpiLC transition (Figure S7D). Additionally, consistent with the lack of GRHL2 expression in ESCs and absence of morphological changes in GRHL2 KO ESCs, the expression of epithelial and mesenchymal markers was unchanged in GRHL2 KO ESCs (Figures S7E). Therefore, morphological, enhancer, and gene expression changes were all consistent with GRHL2 functioning in the maintenance of an epithelial state in EpiLCs. Together, these results show that GRHL2 replaces naive factors in EpiLCs to regulate a subset of the naive pluripotency network that drives an epithelial program largely shared between the naive and formative pluripotent states.

DISCUSSION

Here, we identify a TF, GRHL2, that plays a key role in rewiring enhancers during the ESC to EpiLC transition with minimal transcriptional changes. GRHL2 binding to its target sites in EpiLCs is both necessary and sufficient to fully activate latent enhancers. In the absence of GRHL2 in EpiLCs, a number of genes closest to these sites within the same TAD show reduced expression. However, these genes are already expressed at similar levels in ESCs and exhibit small changes in expression during the ESC to EpiLC transition. At least in part, the lack of major expression changes is due to the presence of alternative enhancers driven by TFs specific to naive ESCs, such as members of the KLF family. These enhancers are becoming inactivated just as the GRHL2 target enhancers are becoming activated. Given that GRHL2 only targets a very small subset of genes driven by the naive pluripotency network, we propose that it is part of a larger group of EpiLC TFs that assume control of the naive pluripotency program as cells of the epiblast prepare for lineage diversification (Figure 7D).

In support of the GRHL2-bound enhancers functioning specifically in EpiLCs, analysis of recently published promoter capture HiC data showed very few significant interactions between GRHL2 enhancers and predicted target genes in ESCs (Novo et al., 2018). However, interpretation of this finding is limited by the ability of the assay to robustly detect enhancer-promoter interactions that are in close linear proximity or that are not super-enhancers. We unfortunately could not confirm the presence of these enhancer-promoter interactions in promoter capture HiC data in EpiSCs from the same study, as GRHL2 is not expressed in EpiSCs (Factor et al., 2014).

While it is widely known that genes can be driven by distinct enhancers in different tissues and developmental stages, there are few known examples of changes in enhancer usage during a continuous developmental transition where a gene stays relatively constantly expressed. One example is the *Oct4* gene, whose regulation is thought to switch from a distal to proximal enhancer during the transition from the early to late epiblast (Yeom et al., 1996). More recently, global profiling of histone marks in naive ESCs versus primed EpiSCs suggested extensive enhancer switching between these two cell states. However, unlike EpiLCs, EpiSCs are a distinct cell state derived through prolonged passage rather than homogeneous transition of differentiating ESCs and they represent a significantly later developmental stage (Kojima et al., 2014). Importantly, the mechanisms driving enhancer switching and the purpose for genes to undergo enhancer switching during a short developmental window with little change in gene expression remain unclear. The results presented here support a regulatory mechanism where a naive and a formative pluripotency TF coordinate enhancer switching to maintain an epithelial program required in both states.

GRHL2 and other GRHL family members have been shown to be key regulators of the epithelial state during development (Pyrgaki et al., 2011; Ray and Niswander, 2016; Werth et al., 2010). They have also been shown to play a role in cancer progression. Tumors with loss-of-function mutations in GRHL proteins often correlate with an epithelial to mesenchymal transition, leading to metastasis (Chung et al., 2016; Cieply et al., 2012, 2013; Werner et al., 2013; Xiang et al., 2012). GRHL2 KO mice have the most severe phenotype of the three Grainyhead proteins, resulting in embryonic lethality by embryonic day 9.5 (E9.5) or E11.5, depending on the mouse strain (Pyrgaki et al., 2011; Rifat et al., 2010; Werth et al., 2010). Those that survive past E9.5 have defects in fusion of a variety of tissues and organs, including an open neural tube and lung and heart defects. These overt phenotypes are likely preceded several days by molecular defects, especially given the molecular changes seen in the GRHL2 KO EpiLCs. *In vitro*, we show a partial epithelial to mesenchymal transition associated with the loss of GRHL2, including a partial downregulation of epithelial genes and upregulation of mesenchymal genes. For example, there was ~50% reduction in E-cadherin expression in the GRHL2 KO EpiLCs. These changes may not be enough to completely deregulate an epithelial to mesenchymal transition during gastrulation and/or there could be additional redundant pathways *in vivo*, explaining the slightly later overt phenotypes.

Previous work on the regulation of 3D architecture by cohesin have focused on long range interactions that form TADs, which are larger loop structures that partition the genome into insulated regulatory units. Enhancers are contained within TADs and are often restricted to activating genes within the same TAD (Dowen et al., 2014; Ji et al., 2016; Mumbach et al., 2016). TAD boundaries are marked by cohesin and the sequence-specific factor CTCF and are largely similar in different cell types (Dixon et al., 2012). Enhancer-promoter interactions that occur within TADs are much more dynamic across cell types and therefore require regulation by different sequence-specific factors in different cell types (Ji et al., 2016). Here, we aimed to identify sequence-specific factors that regulate cohesin localization to new enhancers during differentiation to the EpiLC state. We originally focused on GRHL2 as a TF that may regulate this process. While we found that GRHL2 is indeed necessary and sufficient for cohesin binding at target enhancers, it is also necessary and sufficient for nucleosome removal and deposition of H3K4me1 and H3K27ac. It is unclear whether GRHL2 is required for each of these events or functions early in the process to initiate a cascade of events.

One of the earliest events in enhancer activation is removal of nucleosomes from the enhancer, allowing other TFs to bind (Calo and Wysocka, 2013). Our ATAC-seq data showed that GRHL2 target sites are mostly nucleosome-occluded in ESCs, yet GRHL2 overexpression is able to fully activate these enhancers. GRHL2 overexpression in ESCs also led to binding and activation of many additional sites that are not native GRHL2 binding sites in the EpiLC state. These results suggest a possible role for GRHL2 as a pioneer factor, binding

nucleosome-occluded DNA and opening up the enhancer region. However, GRHL2 may not be functioning alone but could instead be interacting with other TFs that are expressed in both naive and formative states to cooperatively bind and activate its target sites. For example, GRHL2 has been shown to interact with the pioneer TF, FOXA1, which recruits MLL3 to enhancer binding sites in MCF7 cells (Jozwik et al., 2016). Biochemical experiments to identify candidate collaborative factors and acute depletion of these factors will be required to answer this question.

Our findings raise the question of why these cells have evolved such a complex mechanism to simply maintain gene expression. Given that ESCs and EpiLCs are both pluripotent, it is not surprising that they express many of the same genes and at similar levels. However, it is less obvious why these genes are controlled by distinct enhancers in the two states. We propose that the large naive pluripotency network must be subdivided into smaller networks in preparation for lineage specification to form the three germinal layers during gastrulation (Figure 7D). That is, by partitioning genes into smaller networks, their regulation becomes uncoupled, providing EpiLCs with more flexibility to differentiate into these distinct cell fates. GRHL2 regulates just one of these subnetworks (one important in maintaining an epithelial state characteristic of downstream ectoderm cells). Consistent with this model, analysis of single-cell RNA-seq data from the E6.5 gastrulating embryo (Scialdone et al., 2016) shows a positive correlation between expression of GRHL2 and markers of anterior epiblast cells that give rise to ectoderm and a negative correlation with markers of the posterior epiblast and primitive streak that give rise to mesendoderm (Figure S7F). We therefore speculate that a more general mechanism exists where different EpiLC TFs take over regulation of multiple distinct networks to allow for precise control of cell fate as the embryo prepares for gastrulation.

STAR★METHODS

Detailed methods are provided in the online version of this paper and include the following:

- KEY RESOURCES TABLE
- CONTACT FOR REAGENT AND RESOURCE SHARING
- EXPERIMENTAL MODEL AND SUBJECT DETAILS
  - Cell culture conditions
- METHOD DETAILS
  - Targeting of GRHL2 knockout and overexpression lines
  - KLF2 and KLF4 knockout ESC generation
  - Generation of enhancer deletions
  - ChIP-seq
  - ATAC-seq
  - Antibodies
  - ChIP-seq and ATAC-seq data analysis
  - Microarray profiling
  - RNA-seq library preparation and analysis
  - Western blotting
  - Quantitative RT-PCR
- QUANTIFICATION AND STATISTICAL ANALYSIS
- DATA AND SOFTWARE AVAILABILITY

SUPPLEMENTAL INFORMATION

Supplemental Information includes seven figures and seven tables and can be found with this article online at https://doi.org/10.1016/j.stem.2018.06.005.

ACKNOWLEDGMENTS

We thank the UCSF Institute for Human Genetics for technical support and use of their sonicator. We thank Archana Shenoy, Deniz Goekbuget, and Ryan Boileau for critical reading of the manuscript. We thank Dr. Stephen Jane of Monash University for providing the GRHL2 construct. This work was funded by the NIH (grants R01 GM101180 and R01 GM122439 to R.B.). A.F.C. was funded by a California Institute of Regenerative Medicine predoctoral fellowship (TG2-01153). R.K. was funded by the A.P. Giannini Foundation postdoctoral fellowship.

AUTHOR CONTRIBUTIONS

A.F.C. and R.B. conceived the project. A.F.C. designed and performed the experiments and data analysis. A.J.L. contributed to Figures 1D, 7B, 7C, S1B, S1C, S2D, S3B, and S7D. R.K. performed ATAC-seq and contributed to Figure S1A. J.W.F. contributed to Figures 4B, 4C, S4A, S4F, and S5A. B.D. contributed to Figure S7F. A.F.C. and R.B. wrote the manuscript.

DECLARATION OF INTERESTS

The authors declare no competing interests.

Received: January 17, 2017
Revised: December 17, 2017
Accepted: June 10, 2018
Published: July 12, 2018

REFERENCES

Auclair, G., Guibert, S., Bender, A., and Weber, M. (2014). Ontogeny of CpG island methylation and specificity of DNMT3 methyltransferases during embryonic development in the mouse. Genome Biol. *15*, 545.

Beard, C., Hochedlinger, K., Plath, K., Wutz, A., and Jaenisch, R. (2006). Efficient method to generate single-copy transgenic mice by site-specific integration in embryonic stem cells. Genesis *44*, 23–28.

Bedzhov, I., and Zernicka-Goetz, M. (2014). Self-organizing properties of mouse pluripotent cells initiate morphogenesis upon implantation. Cell *156*, 1032–1044.

Bogdanovic, O., Fernandez-Miñán, A., Tena, J.J., de la Calle-Mustienes, E., Hidalgo, C., van Kruysbergen, I., van Heeringen, S.J., Veenstra, G.J., and Gómez-Skarmeta, J.L. (2012). Dynamics of enhancer chromatin signatures mark the transition from pluripotency to cell specification during embryogenesis. Genome Res. *22*, 2043–2053.

Boglev, Y., Wilanowski, T., Caddy, J., Parekh, V., Auden, A., Darido, C., Hislop, N.R., Cangkrama, M., Ting, S.B., and Jane, S.M. (2011). The unique and cooperative roles of the Grainy head-like transcription factors in epidermal development reflect unexpected target gene specificity. Dev. Biol. *349*, 512–522.

Bonn, S., Zinzen, R.P., Girardot, C., Gustafson, E.H., Perez-Gonzalez, A., Delhomme, N., Ghavi-Helm, Y., Wilczyński, B., Riddell, A., and Furlong, E.E.M. (2012). Tissue-specific analysis of chromatin state identifies temporal signatures of enhancer activity during embryonic development. Nat. Genet. *44*, 148–156.

Borgel, J., Guibert, S., Li, Y., Chiba, H., Schübeler, D., Sasaki, H., Forné, T., and Weber, M. (2010). Targets and dynamics of promoter DNA methylation during early mouse development. Nat. Genet. *42*, 1093–1100.

Boroviak, T., Loos, R., Lombard, P., Okahara, J., Behr, R., Sasaki, E., Nichols, J., Smith, A., and Bertone, P. (2015). Lineage-specific profiling delineates the emergence and progression of naive pluripotency in mammalian embryogenesis. Dev. Cell *35*, 366–382.

Buecker, C., Srinivasan, R., Wu, Z., Calo, E., Acampora, D., Faial, T., Simeone, A., Tan, M., Swigut, T., and Wysocka, J. (2014). Reorganization of enhancer

patterns in transition from naive to primed pluripotency. Cell Stem Cell *14*, 838–853.

Buenrostro, J.D., Giresi, P.G., Zaba, L.C., Chang, H.Y., and Greenleaf, W.J. (2013). Transposition of native chromatin for fast and sensitive epigenomic profiling of open chromatin, DNA-binding proteins and nucleosome position. Nat. Methods *10*, 1213–1218.

Buenrostro, J.D., Wu, B., Chang, H.Y., and Greenleaf, W.J. (2015). ATAC-seq: a method for assaying chromatin accessibility genome-wide. Curr. Protoc. Mol. Biol *109*, 1–9.

Calo, E., and Wysocka, J. (2013). Modification of enhancer chromatin: what, how, and why? Mol. Cell *49*, 825–837.

Chen, E.Y., Tan, C.M., Kou, Y., Duan, Q., Wang, Z., Meirelles, G.V., Clark, N.R., and Ma'ayan, A. (2013). Enrichr: interactive and collaborative HTML5 gene list enrichment analysis tool. BMC Bioinformatics *14*, 128.

Chung, V.Y., Tan, T.Z., Tan, M., Wong, M.K., Kuay, K.T., Yang, Z., Ye, J., Muller, J., Koh, C.M., Guccione, E., et al. (2016). GRHL2-miR-200-ZEB1 maintains the epithelial status of ovarian cancer through transcriptional regulation and histone modification. Sci. Rep. *6*, 19943.

Cieply, B., Riley, P., 4th, Pifer, P.M., Widmeyer, J., Addison, J.B., Ivanov, A.V., Denvir, J., and Frisch, S.M. (2012). Suppression of the epithelial-mesenchymal transition by Grainyhead-like-2. Cancer Res. *72*, 2440–2453.

Cieply, B., Farris, J., Denvir, J., Ford, H.L., and Frisch, S.M. (2013). Epithelial-mesenchymal transition and tumor suppression are controlled by a reciprocal feedback loop between ZEB1 and Grainyhead-like-2. Cancer Res. *73*, 6299–6309.

Creyghton, M.P., Cheng, A.W., Welstead, G.G., Kooistra, T., Carey, B.W., Steine, E.J., Hanna, J., Lodato, M.A., Frampton, G.M., Sharp, P.A., et al. (2010). Histone H3K27ac separates active from poised enhancers and predicts developmental state. Proc. Natl. Acad. Sci. USA *107*, 21931–21936.

Dixon, J.R., Selvaraj, S., Yue, F., Kim, A., Li, Y., Shen, Y., Hu, M., Liu, J.S., and Ren, B. (2012). Topological domains in mammalian genomes identified by analysis of chromatin interactions. Nature *485*, 376–380.

Dobin, A., Davis, C.A., Schlesinger, F., Drenkow, J., Zaleski, C., Jha, S., Batut, P., Chaisson, M., and Gingeras, T.R. (2013). STAR: ultrafast universal RNA-seq aligner. Bioinformatics *29*, 15–21.

Dowen, J.M., Fan, Z.P., Hnisz, D., Ren, G., Abraham, B.J., Zhang, L.N., Weintraub, A.S., Schujiers, J., Lee, T.I., Zhao, K., and Young, R.A. (2014). Control of cell identity genes occurs in insulated neighborhoods in mammalian chromosomes. Cell *159*, 374–387.

Factor, D.C., Corradin, O., Zentner, G.E., Saiakhova, A., Song, L., Chenoweth, J.G., McKay, R.D., Crawford, G.E., Scacheri, P.C., and Tesar, P.J. (2014). Epigenomic comparison reveals activation of "seed" enhancers during transition from naive to primed pluripotency. Cell Stem Cell *14*, 854–863.

Hayashi, K., Ohta, H., Kurimoto, K., Aramaki, S., and Saitou, M. (2011). Reconstitution of the mouse germ cell specification pathway in culture by pluripotent stem cells. Cell *146*, 519–532.

Heinz, S., Benner, C., Spann, N., Bertolino, E., Lin, Y.C., Laslo, P., Cheng, J.X., Murre, C., Singh, H., and Glass, C.K. (2010). Simple combinations of lineage-determining transcription factors prime cis-regulatory elements required for macrophage and B cell identities. Mol. Cell *38*, 576–589.

Ji, X., Dadon, D.B., Powell, B.E., Fan, Z.P., Borges-Rivera, D., Shachar, S., Weintraub, A.S., Hnisz, D., Pegoraro, G., Lee, T.I., et al. (2016). 3D chromosome regulatory landscape of human pluripotent cells. Cell Stem Cell *18*, 262–275.

Johnson, W.E., Li, C., and Rabinovic, A. (2007). Adjusting batch effects in microarray expression data using empirical Bayes methods. Biostatistics *8*, 118–127.

Jozwik, K.M., Chernukhin, I., Serandour, A.A., Nagarajan, S., and Carroll, J.S. (2016). FOXA1 directs H3K4 monomethylation at enhancers via recruitment of the methyltransferase MLL3. Cell Rep. *17*, 2715–2723.

Kagey, M.H., Newman, J.J., Bilodeau, S., Zhan, Y., Orlando, D.A., van Berkum, N.L., Ebmeier, C.C., Goossens, J., Rahl, P.B., Levine, S.S., et al. (2010). Mediator and cohesin connect gene expression and chromatin architecture. Nature *467*, 430–435.

Kim, T.H., Abdullaev, Z.K., Smith, A.D., Ching, K.A., Loukinov, D.I., Green, R.D., Zhang, M.Q., Lobanenkov, V.V., and Ren, B. (2007). Analysis of the vertebrate insulator protein CTCF-binding sites in the human genome. Cell *128*, 1231–1245.

Kojima, Y., Kaufman-Francis, K., Studdert, J.B., Steiner, K.A., Power, M.D., Loebel, D.A., Jones, V., Hor, A., de Alencastro, G., Logan, G.J., et al. (2014). The transcriptional and functional properties of mouse epiblast stem cells resemble the anterior primitive streak. Cell Stem Cell *14*, 107–120.

Krishnakumar, R., Chen, A.F., Pantovich, M.G., Danial, M., Parchem, R.J., Labosky, P.A., and Blelloch, R. (2016). FOXD3 regulates pluripotent stem cell potential by simultaneously initiating and repressing enhancer activity. Cell Stem Cell *18*, 104–117.

Kuleshov, M.V., Jones, M.R., Rouillard, A.D., Fernandez, N.F., Duan, Q., Wang, Z., Koplev, S., Jenkins, S.L., Jagodnik, K.M., Lachmann, A., et al. (2016). Enrichr: a comprehensive gene set enrichment analysis web server 2016 update. Nucleic Acids Res. *44* (W1), W90-7.

Langmead, B., and Salzberg, S.L. (2012). Fast gapped-read alignment with Bowtie 2. Nat. Methods *9*, 357–359.

Li, H., Handsaker, B., Wysoker, A., Fennell, T., Ruan, J., Homer, N., Marth, G., Abecasis, G., and Durbin, R.; 1000 Genome Project Data Processing Subgroup (2009). The sequence alignment/map format and SAMtools. Bioinformatics *25*, 2078–2079.

Liao, Y., Smyth, G.K., and Shi, W. (2014). featureCounts: an efficient general purpose program for assigning sequence reads to genomic features. Bioinformatics *30*, 923–930.

Liu, Y., Pelham-Webb, B., Di Giammartino, D.C., Li, J., Kim, D., Kita, K., Saiz, N., Garg, V., Doane, A., Giannakakou, P., et al. (2017). Widespread mitotic bookmarking by histone marks and transcription factors in pluripotent stem cells. Cell Rep. *19*, 1283–1293.

Love, M.I., Huber, W., and Anders, S. (2014). Moderated estimation of fold change and dispersion for RNA-seq data with DESeq2. Genome Biol. *15*, 550.

McLean, C.Y., Bristor, D., Hiller, M., Clarke, S.L., Schaar, B.T., Lowe, C.B., Wenger, A.M., and Bejerano, G. (2010). GREAT improves functional interpretation of cis-regulatory regions. Nat. Biotechnol. *28*, 495–501.

Mumbach, M.R., Rubin, A.J., Flynn, R.A., Dai, C., Khavari, P.A., Greenleaf, W.J., and Chang, H.Y. (2016). HiChIP: efficient and sensitive analysis of protein-directed genome architecture. Nat. Methods *13*, 919–922.

Nakamura, T., Okamoto, I., Sasaki, K., Yabuta, Y., Iwatani, C., Tsuchiya, H., Seita, Y., Nakamura, S., Yamamoto, T., and Saitou, M. (2016). A developmental coordinate of pluripotency among mice, monkeys and humans. Nature *537*, 57–62.

Nichols, J., and Smith, A. (2009). Naive and primed pluripotent states. Cell Stem Cell *4*, 487–492.

Nichols, J., and Smith, A. (2012). Pluripotency in the embryo and in culture. Cold Spring Harb. Perspect. Biol. *4*, a008128.

Novo, C.L., Javierre, B.-M., Cairns, J., Segonds-Pichon, A., Wingett, S.W., Freire-Pritchett, P., Furlan-Magaril, M., Schoenfelder, S., Fraser, P., and Rugg-Gunn, P.J. (2018). Long-range enhancer interactions are prevalent in mouse embryonic stem cells and are reorganized upon pluripotent state transition. Cell Rep. *22*, 2615–2627.

Parchem, R.J., Ye, J., Judson, R.L., LaRussa, M.F., Krishnakumar, R., Blelloch, A., Oldham, M.C., and Blelloch, R. (2014). Two miRNA clusters reveal alternative paths in late-stage reprogramming. Cell Stem Cell *14*, 617–631.

Phillips-Cremins, J.E., Sauria, M.E., Sanyal, A., Gerasimova, T.I., Lajoie, B.R., Bell, J.S., Ong, C.T., Hookway, T.A., Guo, C., Sun, Y., et al. (2013). Architectural protein subclasses shape 3D organization of genomes during lineage commitment. Cell *153*, 1281–1295.

Pyrgaki, C., Liu, A., and Niswander, L. (2011). Grainyhead-like 2 regulates neural tube closure and adhesion molecule expression during neural fold fusion. Dev. Biol. *353*, 38–49.

Quinlan, A.R., and Hall, I.M. (2010). BEDTools: a flexible suite of utilities for comparing genomic features. Bioinformatics *26*, 841–842.

Rada-Iglesias, A., Bajpai, R., Swigut, T., Brugmann, S.A., Flynn, R.A., and Wysocka, J. (2011). A unique chromatin signature uncovers early developmental enhancers in humans. Nature *470*, 279–283.

Ramírez, F., Ryan, D.P., Grüning, B., Bhardwaj, V., Kilpert, F., Richter, A.S., Heyne, S., Dündar, F., and Manke, T. (2016). deepTools2: a next generation web server for deep-sequencing data analysis. Nucleic Acids Res. *44* (W1), W160-5.

Rastan, S. (1982). Timing of X-chromosome inactivation in postimplantation mouse embryos. J. Embryol. Exp. Morphol. *71*, 11–24.

Ray, H.J., and Niswander, L.A. (2016). Grainyhead-like 2 downstream targets act to suppress epithelial-to-mesenchymal transition during neural tube closure. Development *143*, 1192–1204.

Rifat, Y., Parekh, V., Wilanowski, T., Hislop, N.R., Auden, A., Ting, S.B., Cunningham, J.M., and Jane, S.M. (2010). Regional neural tube closure defined by the Grainy head-like transcription factors. Dev. Biol. *345*, 237–245.

Rossant, J., and Tam, P.P.L. (2009). Blastocyst lineage formation, early embryonic asymmetries and axis patterning in the mouse. Development *136*, 701–713.

Schoenfelder, S., Furlan-Magaril, M., Mifsud, B., Tavares-Cadete, F., Sugar, R., Javierre, B.-M., Nagano, T., Katsman, Y., Sakthidevi, M., Wingett, S.W., et al. (2015). The pluripotent regulatory circuitry connecting promoters to their long-range interacting elements. Genome Res. *25*, 582–597.

Scialdone, A., Tanaka, Y., Jawaid, W., Moignard, V., Wilson, N.K., Macaulay, I.C., Marioni, J.C., and Göttgens, B. (2016). Resolving early mesoderm diversification through single-cell expression profiling. Nature *535*, 289–293.

Smith, A. (2017). Formative pluripotency: the executive phase in a developmental continuum. Development *144*, 365–373.

Werner, S., Frey, S., Riethdorf, S., Schulze, C., Alawi, M., Kling, L., Vafaizadeh, V., Sauter, G., Terracciano, L., Schumacher, U., et al. (2013). Dual roles of the transcription factor grainyhead-like 2 (GRHL2) in breast cancer. J. Biol. Chem. *288*, 22993–23008.

Werth, M., Walentin, K., Aue, A., Schönheit, J., Wuebken, A., Pode-Shakked, N., Vilianovitch, L., Erdmann, B., Dekel, B., Bader, M., et al. (2010). The transcription factor grainyhead-like 2 regulates the molecular composition of the epithelial apical junctional complex. Development *137*, 3835–3845.

Xiang, X., Deng, Z., Zhuang, X., Ju, S., Mu, J., Jiang, H., Zhang, L., Yan, J., Miller, D., and Zhang, H.-G. (2012). Grhl2 determines the epithelial phenotype of breast cancers and promotes tumor progression. PLoS ONE *7*, e50781.

Yeom, Y.I., Fuhrmann, G., Ovitt, C.E., Brehm, A., Ohbo, K., Gross, M., Hübner, K., and Schöler, H.R. (1996). Germline regulatory element of Oct-4 specific for the totipotent cycle of embryonal cells. Development *122*, 881–894.

Zhang, Y., Liu, T., Meyer, C.A., Eeckhoute, J., Johnson, D.S., Bernstein, B.E., Nusbaum, C., Myers, R.M., Brown, M., Li, W., and Liu, X.S. (2008). Model-based analysis of ChIP-seq (MACS). Genome Biol. *9*, R137.

STAR★METHODS

KEY RESOURCES TABLE

REAGENT or RESOURCE	SOURCE	IDENTIFIER
Antibodies		
Normal Rabbit IgG	Invitrogen	Cat#10500C
Rabbit anti-H3K4me1	Abcam	Cat#ab8895; RRID:AB_306847
Rabbit Anti-H3K27Ac	Abcam	Cat #ab4729; RRID:AB_2118291
Rabbit anti-SMC1	Bethyl	Cat #A300-055A; RRID:AB_2192467
Rabbit anti-HA tag	Abcam	Cat #ab9110; RRID:AB_307019
Rabbit anti-GRHL2	Sigma	Cat #HPA004820; RRID:AB_1857928
Mouse anti-TATA binding protein	Abcam	Cat #ab5184; RRID:AB_945758
Goat anti-KLF4	R&D	Cat #AF3158; RRID:AB_2130245
Rabbit anti-KLF2	Millipore	Cat #09-820; RRID:AB_10807287
Chemicals, Peptides, and Recombinant Proteins		
MEK inhibitor PD0325901	Peprotech	Cat#3911091
GSK3 inhibitor CHIR99021	Peprotech	Cat#2520691
Critical Commercial Assays		
Nextera DNA Library Prep Kit	Illumina	Cat#FC-121-1030
Deposited Data		
Microarray and sequencing data	This paper	GEO: GSE93147
Experimental Models: Cell Lines		
V6.5 mouse embryonic stem cells containing *miR290*-mCherry and *miR302*-GFP reporters	Parchem et al., 2014	N/A
V6.5 mouse embryonic stem cells containing *Rosa26*-m2rtta; *Col1a1*-FRT	Beard et al., 2006	N/A
Oligonucleotides		
See Table S7 for primer and sgRNA sequences	This paper	N/A
Recombinant DNA		
Cas9 nickase 2A-GFP plasmid	Addgene	Cat#48140
Cas9 nuclease 2A-GFP plasmid	Addgene	Cat#48138
Pgk-ATG-FRT plasmid	Addgene	Cat#20734
Software and Algorithms		
Bowtie2 v2.2.3	Langmead and Salzberg, 2012	http://bowtie-bio.sourceforge.net/bowtie2/index.shtml
Samtools v1.5	Li et al., 2009	http://samtools.sourceforge.net/
Bedtools v2.17.0	Quinlan and Hall 2010	https://github.com/arq5x/bedtools2
Deeptools v2.5.7	Ramírez et al., 2016	https://github.com/deeptools/deepTools/
Homer	Heinz et al., 2010	http://homer.ucsd.edu/homer/index.html
STAR v2.5.3a	Dobin et al., 2013	https://github.com/alexdobin/STAR
DESeq2	Love et al., 2014	https://bioconductor.org/packages/release/bioc/html/DESeq2.html
Featurecounts v1.5.3	Liao et al., 2014	http://bioinf.wehi.edu.au/featureCounts/
R v3.4.2	R Core Team	https://www.r-project.org/
MACS2 v2.1.0	Zhang et al., 2008	https://github.com/taoliu/MACS

CONTACT FOR REAGENT AND RESOURCE SHARING

Further information and requests for resources and reagents should be directed to and will be fulfilled by the Lead Contact, Robert Blelloch (robert.blelloch@ucsf.edu).

EXPERIMENTAL MODEL AND SUBJECT DETAILS

Cell culture conditions

V6.5 ESCs were cultured in Knockout DMEM (Invitrogen) supplemented with 15% FBS, LIF (1000U/mL), and 2i (1uM MEK inhibitor PD0325901 and 3uM GSK3 inhibitor CHIR99021). EpiLCs were generated by removal of LIF and 2i as described in Krishnakumar et al., 2016. Briefly, 400,000 ESCs were plated per 15cm plate on day −1 in ESC media. To initiate differentiation, LIF and 2i were removed approximately 24 hours after seeding (day 0). EpiLCs were collected on day 3 of differentiation, approximately 65 hours after removal of LIF and 2i. GRHL2 expression was induced in the dox-inducible *Rosa26*-M2rtTA; TetO-HA-GRHL2 ESCs with 0.5ug/mL final concentration of doxycycline for 24 hours prior to collection for ChIP-seq.

METHOD DETAILS

Targeting of GRHL2 knockout and overexpression lines

GRHL2 knockout ESCs were generated using clustered regularly interspaced short palindromic repeats (CRISPR) technology roughly as described in Ran et al., 2013. Pairs of guide RNAs compatible for Cas9 nicking were designed against exon 2 of *Grhl2* using the CRISPR Design Tool (http://crispr.mit.edu/). Each guide RNA was cloned into a plasmid containing Cas9 nickase-2A-GFP (Addgene plasmid ID: 48140). Paired plasmids were then nucleofected into V6.5 ESCs (Lonza mouse ESC nucleofector kit). GFP positive ESCs were single cell sorted into 96 well plates the next day. Individual clones were genotyped for shifts in PCR product size in both alleles, and the resulting products were gel extracted and sequenced to verify that a truncated protein was generated. Positive clones were expanded and the absence of GRHL2 protein was confirmed by western blot.

ESCs containing dox-inducible HA-tagged GRHL2 were generated using a system developed by Beard et al., 2006. V6.5 ESCs targeted with Rosa26-M2rtTA and a FRT site downstream of the *ColA1* 3′UTR were electroporated with the Pgk-ATG-FRT plasmid (Addgene plasmid #20734) containing HA-GRHL2 cloned into the EcoRI site (Beard et al., 2006). Cells were plated onto irradiated MEFs and selected with hygromycin (140ug/mL) after 24 hours. Surviving clones were genotyped for insertion of the construct at the correct locus and confirmed to induce expression of HA-GRHL2 with addition of 0.5ug/mL doxycycline (Figure S3B).

KLF2 and KLF4 knockout ESC generation

KLF2 and KLF4 double KO ESCs were generated similarly to GRHL2 KO ESCs using CRISPR technology, except that a Cas9 nuclease-2A-GFP (Addgene plasmid #48138) was used. A pair of guides targeting exon 1 of *Klf2* were cloned into the plasmid and introduced into V6.5 ESCs. GFP positive cells were sorted two days later and plated at clonal density for colony picking. Individual clones were genotyped for shifts in product size in both alleles, and the resulting products were gel extracted and sequenced to verify that a truncated protein was generated. Positive clones were expanded and the absence of KLF2 protein was confirmed by western blot. To generate the double knockout, we then introduced a pair of guides targeted at the region flanking exon 3 of *Klf4* into a KLF2 KO line. Individual clones were genotyped and loss of KLF4 protein was verified by western blot.

Generation of enhancer deletions

To generate deletions of individual KLF4 and GRHL2-bound enhancers, we designed pairs of guides spaced approximately 200bp apart surrounding the KLF4 or GRHL2 sequence motif and cloned these into Cas9 nuclease-2A-GFP plasmids (Addgene plasmid #48138). We then expanded GFP-positive clones and genotyped them for shifts in product size for both alleles as described above. Positive clones were then sequenced to verify deletion of the TF sequence motif.

ChIP-seq

Cells were fixed in 1.5mM EGS for 30 mins, and then 1% PFA for 5 mins. Nuclei were isolated using nuclear extraction buffer (5mM PIPES pH 8.0, 85mM KCl, 0.5% NP-40) and lysed in shearing buffer (10mM Tris-HCl pH 7.6, 1mM EDTA, 0.1% SDS). Chromatin was sheared using a Covaris S2 sonicator (Duty cycle: 10%, Intensity: 4, Cycles/burst: 200, Mode: Frequency sweeping, 12 mins) and fragments were verified by gel electrophoresis to be predominantly between 100-500 bp. Antibodies were pre-incubated with a mix of 20ul Protein A and 20ul Protein G Dynabeads (Invitrogen) and then incubated overnight with sheared chromatin under IP conditions (0.5% Tritox X-100, 2mM EDTA, 20mM Tris, 150mM NaCl, 0.1% SDS). Approximately 10 million cells were used per IP. The next day, beads were sequentially washed with the following buffers: Low salt wash buffer (20mM Tris pH 7.9, 2mM EDTA, 125mM NaCl, 0.05% SDS, 1% Triton X-100); High salt wash buffer (20mM Tris pH 7.9, 2mM EDTA, 500mM NaCl, 0.05% SDS, 1% Triton X-100); LiCl wash buffer (10mM Tris pH 7.9, 1mM EDTA, 250mM LiCl, 1% NP-40, 1% sodium deoxycholate); and 1X TE. Immunoprecipitated DNA was then eluted (100mM sodium bicarbonate, 1% SDS) and de-crosslinked overnight at 65°C before being purified. Protease and phosphatase inhibitors were added to each buffer prior to elution. Purified DNA was then used for generation of ChIP-seq libraries as described in Krishnakumar et al., 2016.

ATAC-seq

ATAC-seq libraries were generated as described in (Buenrostro et al., 2015). Briefly, 50000 cells were washed, resuspended in cold lysis buffer, and spun down to pellet nuclei. Isolated nuclei were then resuspended in Tn5 transposase reaction mix from Nextera (Illumina FC-121-1030) and incubated at 37 degrees for 30 mins. The reaction was purified using QIAGEN MinElute columns and then amplified for 8 cycles to produce libraries for sequencing.

Antibodies

Antibodies used for ChIP-seq and/or western blotting are as follows: Normal Rabbit IgG (Invitrogen 10500C, 10ug/IP); H3K4me1 (Abcam ab8895, 5ug/IP), H3K27ac (Abcam ab4729, 5ug/IP), SMC1 (Bethyl A300-055A, 10ug/IP), HA (Abcam ab9110 5ug/IP), GRHL2 (Sigma HPA004820 5ug/IP), TATA-binding protein (Abcam ab51841), KLF4 (R&D AF3158), KLF2 (Millipore 09-820). All antibodies were used at 1:1000 for western blotting.

ChIP-seq and ATAC-seq data analysis

Fastq files were mapped to mm10 using Bowtie 2 (Langmead and Salzberg, 2012) and converted to bam and bed files using samtools (Li et al., 2009) and bedtools (Quinlan and Hall, 2010). Only uniquely mapping (map quality > 30), deduplicated reads were used for analysis. Peaks were identified with MACS2 using the following parameters:–nomodel–extsize 200 -s 50–bw 200 -f BAM -g mm -B -q 0.05. In the case of KLF4 ChIP-seq from Liu et al., a q-value of 5E-5 was used, and only sites containing a KLF motif were considered true KLF4 sites. For SMC1 peaks, an IgG control was used as background. For GRHL2 peaks, a GRHL2 ChIP in GRHL2 knockout cells was used as background. For KLF4, input DNA was used as a background. Metagene analyses were performed as described in Krishnakumar et al., 2016, except a moving average was calculated using a window size of 400bp and a step size of 100bp. Heatmaps of ChIP signal were generated using deepTools2 (Ramírez et al., 2016). Homer was used for motif-finding (Heinz et al., 2010). GREAT was used for GO analysis of likely target genes of GRHL2-bound enhancers. Candidate target genes were assigned based on nearest gene within the same TAD based on TAD boundaries identified in ESCs by Dixon et al., 2012. Two biological replicates were sequenced for each condition and initially analyzed separately to ensure results were consistent between replicates, and then analyses were repeated by combining the reads from each replicate. At least 20 and 7 million uniquely mapping, deduplicated reads were used for ChIP-seq and ATAC-seq analysis per condition, respectively (Table S7). To visualize ChIP-seq tracks at specific loci, bam files were converted to read normalized bedgraph files using bedtools and then converted to bigwig files and uploaded onto the Integrative Genome Viewer from the Broad Institute.

Microarray profiling

Total RNA was Trizol extracted from 4 independent wild-type and GRHL2 knockout clones differentiated into the EpiLC state. RNA was sent to the UCLA Neuroscience Genomics Core for hybridization to the Illumina Mouse Ref 8 v 2.0 Beadchip. Data was quantile normalized using the beadarray package on Bioconductor and differential gene expression in GRHL2 knockout versus wild-type EpiLCs was determined using the limma package.

RNA-seq library preparation and analysis

RNA-seq libraries of KLF2/4 double KO ESCs were generated using the QuantSeq 3′ mRNA-Seq Library Prep Kit FWD for Illumina (Lexogen) as per their protocol. Total RNA was Trizol extracted from four wild-type samples and five KLF2/4 double KO samples (three independent clones; two samples for two clones and one sample for one clone). 600ng of total RNA was used as input for each library. For RNA-seq of ESCs and EpiLCs, RNA was collected using Trizol and rRNA was depleted using the Ribo-Zero Gold kit (Illumina). ~100 ng of rRNA depleted RNA was used as input for the Kapa Stranded RNA-Seq kit (Kapa). Libraries were sequenced on a HiSeq 4000.

Reads were trimmed to remove adaptor sequences using cutadapt and mapped to the genome (mm10) with STAR (Dobin et al., 2013) using the following parameters:–outFilterMultimapNmax 1–outFilterMismatchNoverReadLmax 0.05–seedSearchStartLmax 25–winAnchorMultimapNmax 100. Reads mapping to exons were then counted using featureCounts (Liao et al., 2014). Differential expression analysis was performed using DESeq2 (Love et al., 2014).

For principal component analysis of data from Boroviak et al., 2015, processed Bam files were downloaded from ftp://ftp.ebi.ac.uk/pub/databases/microarray/data/experiment/MTAB/E-MTAB-2958/. Counts were generated using featureCounts v1.5.0 and the mouse Gencode annotation with default options except for strandedness (-s 2). Read count data were used for principal component analysis as follows. First, a count value cutoff of 10 was imposed to remove low-count data (i.e., only genes receiving $\geq$ 10 counts in $\geq$ 1 sample were included in downstream analyses). Count data surpassing this threshold were normalized for total number of counts per sample, as well as for the length of the CDS as measured in base pairs (generating an RPKM-like value). The samples were batch normalized using an empirical Bayes method (Johnson et al., 2007), based on sample source metadata. We used the prcomp function in R, the data were mean-variance scaled, and the results were plotted in 3D (PC1 versus PC2 versus PC3).

Western blotting

Nuclear extracts were prepared by first resuspending cell pellets in cytoplasmic extraction buffer (10mM HEPES, 60mM KCl, 1mM EDTA, 0.075% Igepal, adjusted to pH7.6) to lyse cells and pellet nuclei, and then resuspending nuclei in nuclear extraction buffer (20mM Tris-HCl, 420mM NaCl, 1.5mM MgCl2, 0.2mM EDTA, and 25% glycerol, adjusted to pH 8.0). Nuclear lysates were quantified

and equal amounts of protein were loaded for each sample onto 7.5% Tris-glycine gels. Proteins were transferred onto a PVDF membrane, blocked with Odyssey blocking buffer, and sequentially blotted with primary and secondary antibody. Membranes were then imaged on an Odyssey imaging system (LI-COR)

Quantitative RT-PCR

Trizol extraction was performed to isolate total RNA. RNA was then reverse transcribed using the Superscript III First-strand Synthesis kit or Maxima First Strand cDNA Synthesis kit (Thermofisher). Quantitative PCR reactions were performed using the SensiFAST SYBR Hi-ROX kit (Bioline) or PowerUp SYBR Green Master Mix (Thermofisher) on an ABI 7900HT 384-well PCR machine.

QUANTIFICATION AND STATISTICAL ANALYSIS

Statistical details of experiments can be found in the figure legends, including the statistical test used, value of n, meaning of error bars, and p values. For all figures, the value of n indicates number of biological replicates, defined as distinct dishes of cultured cells. For qPCR experiments, the bar graphs indicate mean of n biological replicates. For microarray and sequencing data, significant differences were defined as an adjusted p value < 0.05, unless otherwise noted in the appropriate Method Details sub-section. Statistical analyses were performed in Microsoft Excel or R.

DATA AND SOFTWARE AVAILABILITY

The accession number for all microarray and sequencing data generated in this paper is GEO: GSE93147.